ACS APPLIED MATERIALS & INTERFACES

Research Article

www.acsami.org

The Positive Roles of Integrated Layered-Spinel Structures Combined with Nanocoating in Low-Cost Li-Rich Cathode $Li[Li_{0.2}Fe_{0.1}Ni_{0.15}Mn_{0.55}]O_2$ for Lithium-Ion Batteries

Taolin Zhao,[†] Shi Chen,[†] Renjie Chen,*[,†,‡] Li Li,[†,‡] Xiaoxiao Zhang,[†] Man Xie,[†] and Feng Wu*[,†,‡]

[†]Beijing Key Laboratory of Environmental Science and Engineering, School of Chemical Engineering and the Environment, Beijing Institute of Technology, Beijing 100081, China

[‡]National Development Center for High Technology Green Materials, Beijing 100081, China

Supporting Information

ABSTRACT: As the most promising cathodes of lithium-ion batteries, lithium-rich manganese-based layered oxides with high capacity suffer from poor cycle stability, poor rate capability, and fast voltage fading. Here we introduced AlF_3 into the surface of layered lithium-rich cathode ($Li[Li_{0.2}Fe_{0.1}Ni_{0.15}Mn_{0.55}]O_2$) as an artificial protective layer as well as an inducer of integrated layered-spinel structures to achieve both low cost and high capacity. The reduced irreversible capacity loss, improved cycling stability, and superior high-rate capability were ascribed to the combination of AlF_3 nanocoating and the unique structures as well as the low charge transfer resistance. Besides, the intractable issue, fast voltage fading of the layered lithium-rich cathode was also alleviated. Such materials with both low cost and high capacity are considered to be promising candidate cathodes to achieve lithium-ion batteries with high energy and high power.

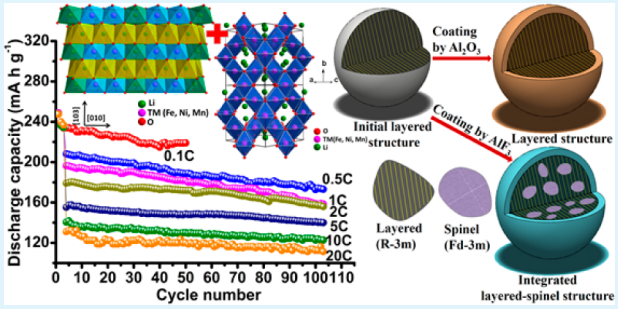

KEYWORDS: *lithium-ion batteries, phase transformation, layered-spinel, AlF_3, nanocoating*

INTRODUCTION

The high reversible capacity (~250 mA h g^{-1}) provided by the promising Li-rich solid solutions between $Li[Li_{1/3}Mn_{2/3}]O_2$ and $LiMO_2$ (M = Fe, Ni, Co, Mn, etc.) can better meet the energy requirement for PHEVs and EVs than the conventional layered $Li[Ni, Co, Mn]O_2$ with a capacity of only 160 mA h g^{-1}.[1−7] However, Co and Ni elements used in representative samples, $Li_2MnO_3{\cdot}LiNi_{0.5}Mn_{0.5}O_2$ and $Li_2MnO_3{\cdot}LiCo_{1/3}Ni_{1/3}Mn_{1/3}O_2$, undoubtedly increase the cost of the whole battery system.[8−12] In recent years, the Fe^{3+}/Fe^{4+} redox couple was observed in the 4 V region of Li-rich materials, such as $Li_{1+x}(Fe_yMn_{1-y})_{1-x}O_2$.[13−18] Therefore, Li-rich cathodes containing Fe element become the research target due to their low cost and environmental friendliness.[19−25] Although a high initial capacity has been achieved, these Fe−Mn based Li-rich materials still suffer from high first irreversible capacity loss, poor cycle stability, and low rate capability. Based on the optimization of synthetic methods and compositional ratios as well as doping or substitution, the low-cost cathodes with high performances have still not been achieved, even the most promising materials $Li_{1+x}[(Fe_{0.5}Ni_{0.5})_yMn_{1-y}]_{1-x}O_2$ ($0 < x < 1/3$, $0.2 \le y \le 0.8$).

The cubic-close-packing in layered and spinel lithium−metal oxide cathodes permits the structural compatibility. Highly stable spinel phase is thought to be promising in improving the rate capabilities of layered oxides because of its three-dimensional interstitial space provided by the $[M_2]O_4$ framework, which is beneficial to the fast diffusion of lithium ions.[26−28] To design low-cost and high-capacity materials with good rate capability, the concept of integrated "layered-spinel" structures was applied on the low-cost Li-rich cathode, $Li[Li_{0.2}Fe_{0.1}Ni_{0.15}Mn_{0.55}]O_2$ (LLFNMO). The compositional phase diagram is shown in Figure S1 (Supporting Information). In addition, nanocoatings, such as aluminum fluoride and aluminum oxide, are also expected to be applied to achieve good cycle stability, which can separate the particles from electrolyte to alleviate decomposition of electrolyte and reduce the side surficial reactions.

To further develop the merits of the integrated "layered-spinel" structures and nanocoating, we combined both of them through a facile "induce strategy" (Scheme 1) to develop a low-cost cathode material with good rate capability and cycle life. The introduction of AlF_3 nanocoating into the surface of cathode material can effectively induce the structural rearrangement to form integrated "layered-spinel" structure.[26,29] Good electrochemical performances can be predicted from the comprehensive design route. First, the AlF_3 nanocoating can separate the host particles from the electrolyte to reduce the

Received: October 10, 2014
Accepted: November 17, 2014
Published: November 17, 2014

Scheme 1. Schematic Diagram for the Synthesis Process

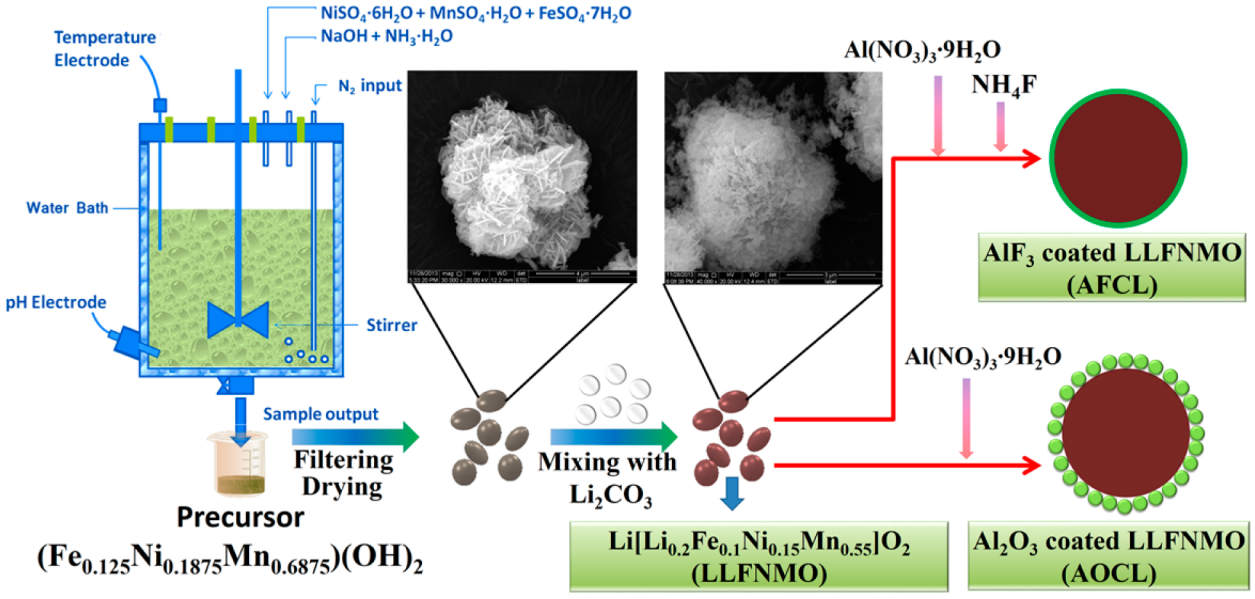

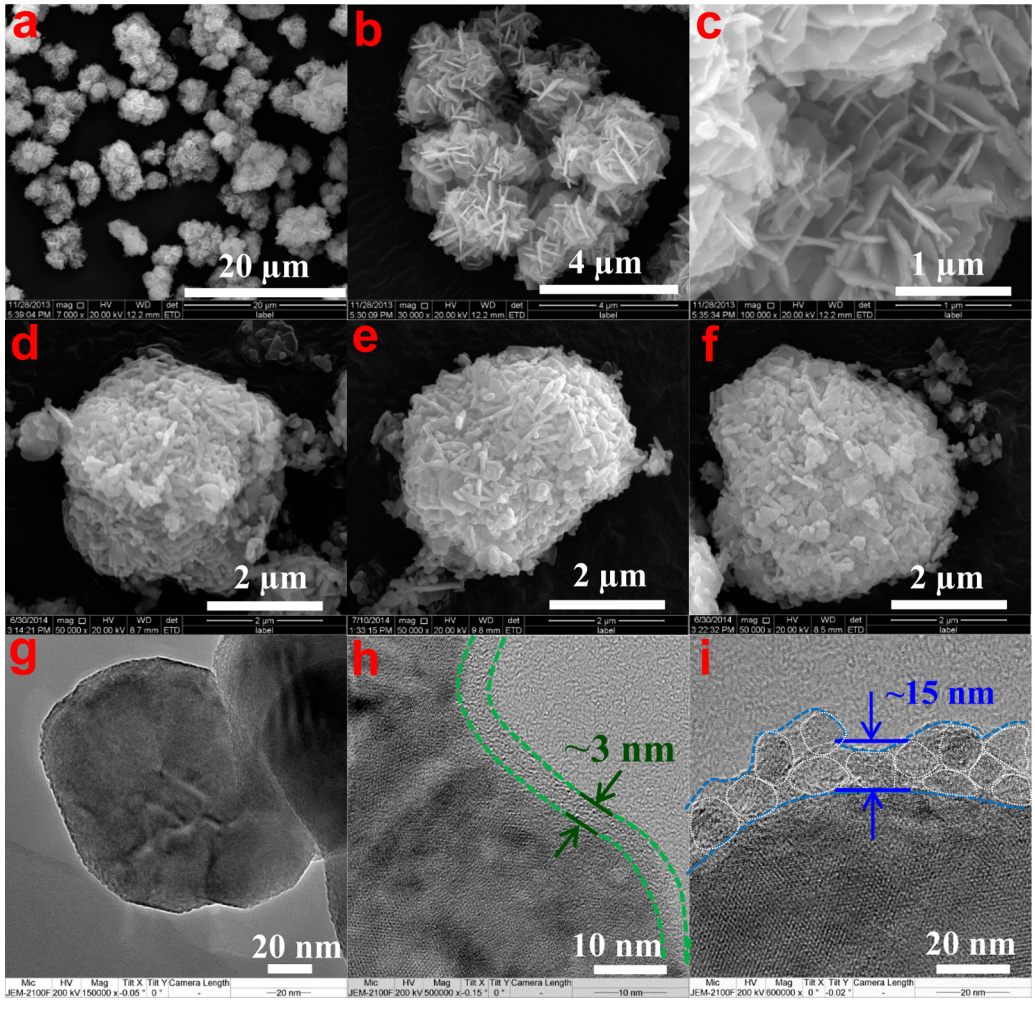

Figure 1. FESEM images of the precursor (a–c), LLFNMO (d), AFCL (e), and AOCL (f); corresponding TEM images of LLFNMO (g), AFCL (h), and AOCL (i).

surficial side reaction as well as alleviate the dissolution of Mn in spinel phase, benefiting the cycle stability. Second, the harmonious coexistence of layered and spinel phase can accelerate lithium ion transportation through independently

dx.doi.org/10.1021/am506934j | ACS Appl. Mater. Interfaces 2014, 6, 21711–21720

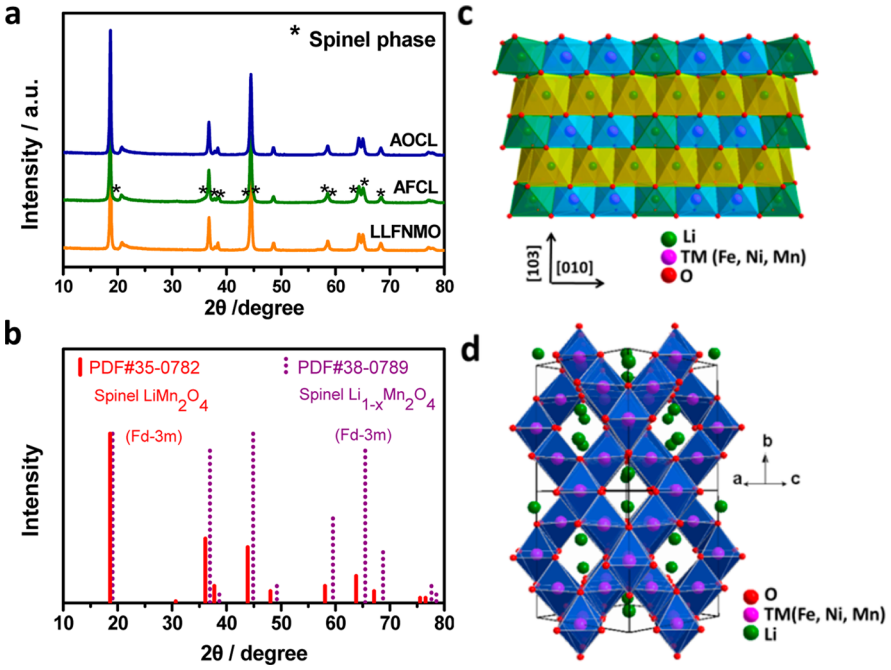

Figure 2. XRD patterns of LLFNMO, AFCL and AOCL (a); Bragg positions for typical spinel $LiMn_2O_4$ and $Li_{1-x}Mn_2O_4$ ($Fd\bar{3}m$) (b); crystal structure of Li-rich layered material ($R\bar{3}m$) (c); crystal structure of cubic spinel phase ($Fd\bar{3}m$) (d).

choosing the fastest and shortest transportation path, ensuring the outstanding rate capability. Also, the induced spinel phase is more stable compared to that formed during cycling in pristine sample. For comparison, Al_2O_3 coated LLFNMO sample (AOCL) was synthesized without observed spinel phases and its electrochemical performances were also investigated systematically to highlight the advantages of the integrated "layered-spinel" material with AlF_3 nanocoating layer (AFCL) and the difference from the spinel phase formation in pristine and AOCL during cycling.

EXPERIMENTAL SECTION

Synthesis of $Li[Li_{0.2}Fe_{0.1}Ni_{0.15}Mn_{0.55}]O_2$. In this work, all the chemicals were of analytical grade and used as-received without further purification. The pristine cathode material $Li[Li_{0.2}Fe_{0.1}Ni_{0.15}Mn_{0.55}]O_2$ was synthesized by coprecipitation method. Nickel sulfate hexahydrate ($NiSO_4{\cdot}6H_2O$), manganese sulfate monohydrate ($MnSO_4{\cdot}H_2O$), iron sulfate heptahydrate ($FeSO_4{\cdot}7H_2O$), sodium hydroxide (NaOH), and ammonium hydroxide ($NH_3{\cdot}H_2O$) were used as starting reagents to prepare the precursor particles $Fe_{0.125}Ni_{0.1875}Mn_{0.6875}(OH)_2$ in a continuously stirred tank reactor (CSTR). During the reaction, 2 M transition metal solution (Fe:Ni:Mn = 0.1:0.15:0.55) was slowly pumped into the reactor. The pH level was kept at 11 by controlling the added amount of the mixture solution of 4 M NaOH and 0.4 M $NH_3{\cdot}H_2O$. The solution was strongly stirred at 1000 rpm. The reaction was conducted under an inert atmosphere by bubbling N_2 into the CSTR to mitigate the oxidation of Mn^{2+} and Ni^{2+}. The spherical precursor was filtered, washed with deionized water, and dried at 100 °C for 48 h. The dried precursor was mixed well with Li_2CO_3 and then calcined at 800 °C for 15 h to obtain the cathode material $Li[Li_{0.2}Fe_{0.1}Ni_{0.15}Mn_{0.55}]O_2$.

Synthesis of AFCL and AOCL Samples. The AlF_3 surface coating layer was obtained as follows: Certain amounts of $Al(NO_3)_3{\cdot}9H_2O$ and NH_4F were dissolved in deionized water. A desired amount of LLFNMO powder was dispersed in the NH_4F solution. The $Al(NO_3)_3{\cdot}9H_2O$ solution was then added into the mixture drop by drop for 3 h. Then, the resulting mixture was heated to 80 °C and stirred vigorously. Continuous stirring was performed until the solution was evaporated to dryness. The obtained powder was calcined at 400 °C in a tube furnace for 5 h in argon gas atmosphere and then cooled to RT to get the AlF_3 coated LLFNMO. The synthesis process of Al_2O_3 coated samples was carried out without NH_4F and calcined at 400 °C in a muffle furnace in air for 5 h.

Material Characterizations. The structure analysis was carried out using X-ray diffraction (XRD; Rigaku Ultima IV-185) with a Cu Kα radiation source. The source tension and current were 40 kV and 40 mA, respectively. Data were acquired with a step size of 0.5° min^{-1} over a 2θ range of 10°−80°. Morphologies of the prepared samples were characterized by a field emission scanning electron microscopy (FESEM, FEI, Quanta 200f) and transmission electron microscopy (TEM, JEM-2100f). Element mappings of the prepared samples were carried out with an energy dispersive X-ray detector (EDX).

Electrochemical Tests. For fabrication of the cathodes, the prepared powders were mixed with acetylene black and polyvinylidene fluoride (8:1:1 by weight) in *N*-methyl-2-pyrrolidone (NMP). The obtained slurry was coated onto Al foil and roll-pressed. The electrodes were dried overnight at 80 °C in a vacuum oven before use. The active mass was ~3 mg. The electrode materials were assembled into 2025 button cells in a glovebox filled with high-purity argon using Li metal as the anode for electrochemical measurements. The electrolyte solution was 1 M $LiPF_6$ in ethyl carbonate (EC) and dimethyl carbonate (DMC) (1:1 by volume). The charge/discharge tests were performed using a Land battery test system (Land CT2001A, Wuhan, China) in the range of 2.0−4.8 V at different current rates with current densities from 20 mA g^{-1} (0.1C) to 4000 mA g^{-1} (20C). A two-step charge process was employed at 0.1C. That is, the constant current charge step was followed by an additional constant voltage charge step until the current density dropped to half of its initial value. Electrochemical impedance spectroscopy (EIS) analysis was carried out from 10^5 to 0.01 Hz using an IM6 electrochemical impedance analyzer with an AC perturbation signal of 5 mV. The potentials throughout the paper are referenced to the Li/Li^+ couple.

RESULTS AND DISCUSSION

Coprecipitation method was employed to synthesize the spherical precursor, $(Fe_{0.125}Ni_{0.1875}Mn_{0.6875})(OH)_2$, with hierarchical structure. The morphologies of the prepared materials, tested by both FESEM and TEM, are shown in Figure 1. The

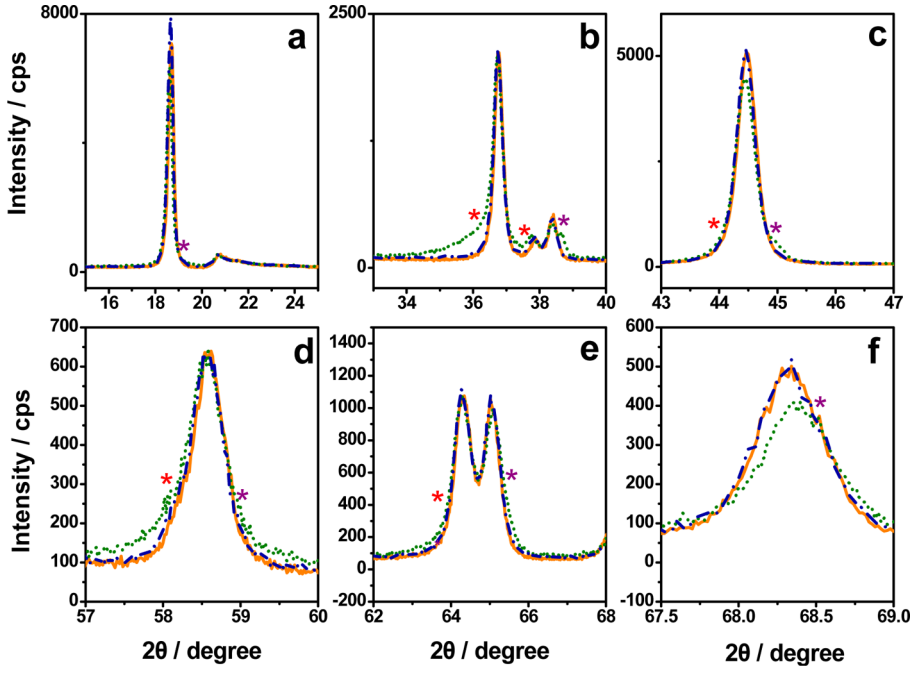

Figure 3. Enlarged view of the XRD patterns for LLFNMO, AFCL, and AOCL samples within a specific 2θ range. (Solid orange, short-dot green, and dash-dot blue lines represent LLFNMO, AFCL, and AOCL samples, respectively. Stars mark out the spinel phases.)

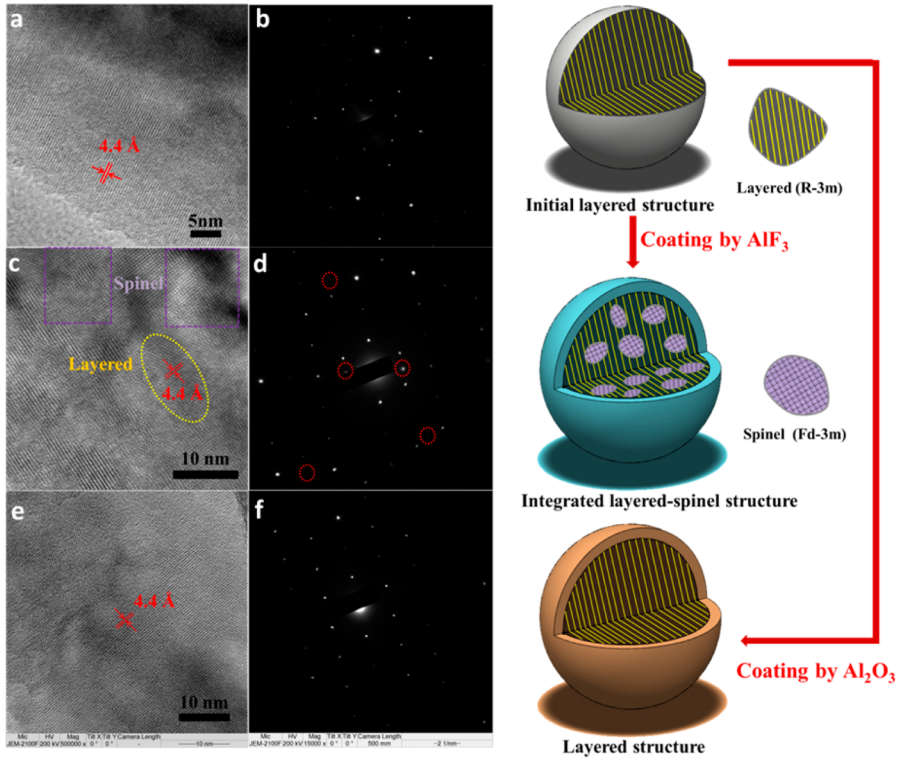

Figure 4. TEM images of LLFNMO (a), AFCL (c), and AOCL (e); corresponding electron diffraction of LLFNMO (b), AFCL (d), and AOCL (f). The right region is the schematic drawing of different structure features.

precursor particles are large agglomerates with 5−6 μm in size (Figure 1a, b), composed of secondary particles formed by polygonal nanoplates with a thickness of 50 nm (Figure 1c). After calcination, the pristine LLFNMO was formed by nanoplates with the thickness of 100 nm (Figure 1d). The surface of LLFNMO is smooth and clean, as shown in TEM image (Figure 1g). After modification by AlF_3 and Al_2O_3, great changes cannot be observed from FESEM images (Figure 1e, f), but from TEM images. Uniform distribution of an amorphous coating layer with a thickness of 3 nm was displayed in the AFCL sample (Figure 1h), while a nanoparticle coating layer (~15 nm) was observed in the AOCL sample (Figure 1i). As for the different microstructures of AlF_3 and Al_2O_3 coatings, calcination atmosphere is considered to be one

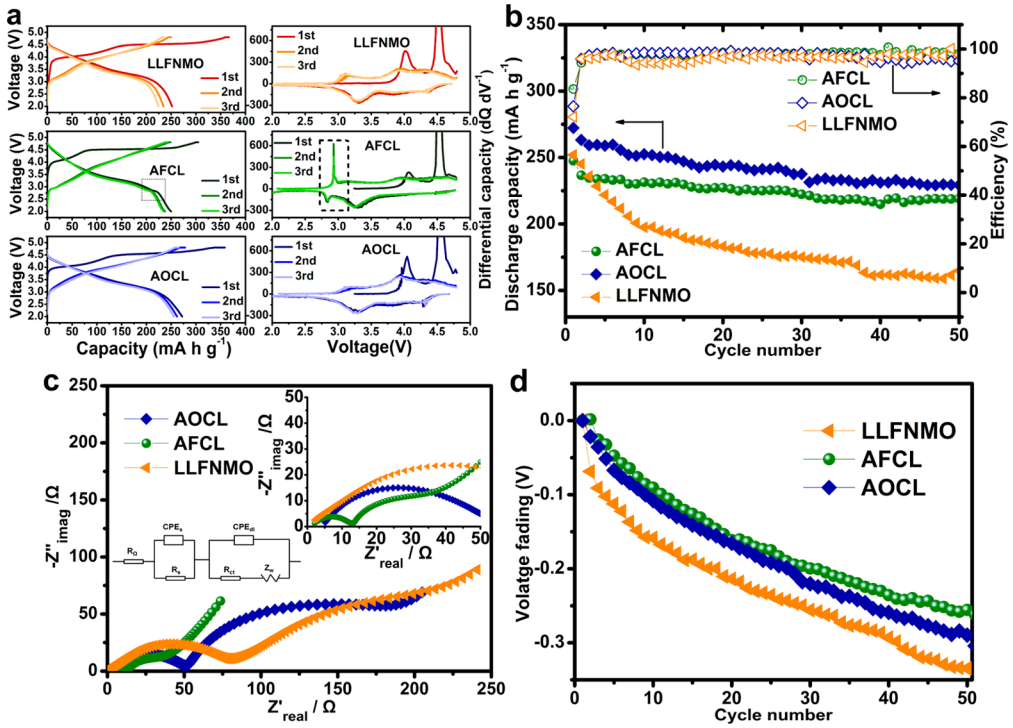

Figure 5. First three charge−discharge curves and the corresponding dQ dV^{-1} versus voltage plots of all three samples (a); cycling stability at 0.1C (b); EIS spectra of all the samples at the charge state of 4.3 V at 50th cycle (c); comparison of voltage fading rates during cycling at 0.1C of all the samples (d).

of the reasons. AlF_3 coating was conducted in the argon atmosphere, while Al_2O_3 coating was carried out in the air atmosphere. In addition, for the synthesis of AlF_3, NH_4F was used as the reactant to provide the source of F element. Also, it acts as a chelating agent and growth promoter to react with Al^{3+} slowly and completely, and thus a thinner and more complete coating layer is obtained. Moreover, the coating amount of Al_2O_3 and AlF_3 are the same as 7%, which is slightly higher than the conventional coating amount, and will cause a little agglomeration in Al_2O_3 coating layer with granular structure. The uniform distribution of elements can be clearly seen in Figure S2 (Supporting Information). The different coating morphologies between the AlF_3 and Al_2O_3 coating layer indicated their different electrochemical performances. As for the AlF_3 coating, the thinner coating layer indicates the more complete coating layer of AlF_3 at the surface of the bulk material. As a result, the AlF_3 coating layer is thought to be more preferred for the electrochemical behaviors than Al_2O_3 coating layer, benefiting from its fine and close texture and thus less contact between bulk material and electrolyte.

The crystal structures of all the samples were identified with X-ray diffraction (XRD) patterns in Figure 2a. No impurity peaks corresponding to the AlF_3-related or Al_2O_3-related compounds were observed. Except the weak superlattice reflection peaks between 20° and 23°, corresponding to the $C/2m$, all the other peaks of LLFNMO can be indexed based on hexagonal α-$NaFeO_2$ structure with space group $R\bar{3}m$ (Figure 2c).[1,30,31] The ordering of metal ions (Li, Fe, Ni and Mn) in the transition metal layer of the layered lattice results in the weak superlattice reflection peaks, which are characteristic of Li-rich Mn-based oxides. As for AOCL sample, its layered structure became better than LLFNMO, indicated by the ratio of (003)/(104) and the splitting of (018)/(110) peaks. However, as for the AlF_3 coated samples, the spinel-related peaks corresponding to $LiMn_2O_4$ or $Li_{1-x}Mn_2O_4$ ($Fd\bar{3}m$) appeared (Figures 2b,d and 3). The obvious shoulder peaks assigned to the $Fd\bar{3}m$ spinel phase have been pointed out by the red star ($LiMn_2O_4$) or purple star ($Li_{1-x}Mn_2O_4$) in Figure 3. All the data clearly confirmed the existence of the $Fd\bar{3}m$ spinel phase in the AFCL sample. These peaks became more evident with the increase of coating amount, especially in 10 wt % AlF_3-coated sample (Figure S3, Supporting Information). The XRD data present that the AlF_3 nanocoating protective layer on the particle surface induces a structure transformation from layer to spinel partially in the host material, while the Al_2O_3 protective layer can effectively improve the layered structure, which can be verified directly by TEM analysis and the electrochemical charge/discharge curves in the following discussion.

The formation of integrated layered-spinel structures was evidenced explicitly by comparative TEM analysis of LLFNMO and AFCL. The different structure features of the three samples are clearly illustrated in Figure 4. An interplanar spacing about 0.44 nm was observed in LLFNMO (Figure 4a), smaller than 0.47 nm of other Li-rich materials without Fe element due to the difference of atomic radius of transition metals. Electron diffraction patterns of the primary particles of LLFNMO matched well with layered Li-rich materials (Figure 4b). However, Figure 4d showed the electron diffraction pattern of AFCL sample indexed to the ⟨110⟩ zone of the cubic spinel structure (corresponding to the purple rectangle region in Figure 4c). The diffraction spots from the spinel structure indicated by the red circles (Figure 4d) are indexed as $(220)_{spinel}$.[15,17,26] As for AOCL, no spinel phase was observed in its TEM image (Figure 4e) and electron diffraction patterns (Figure 4f). Therefore, the comparative images provide clear evidence to verify the presence of integrated layered-spinel structures in AFCL. As reported by other researchers,[32,33] when introducing coating layer into cathode material, the second

dx.doi.org/10.1021/am506934j | ACS Appl. Mater. Interfaces 2014, 6, 21711−21720

Table 1. Initial Charge and Discharge Capacity, and First Cycle Efficiency of All the Samples Cycled between 2.0 and 4.8 V at 0.1C

sample	charge capacity below 4.5 V (mA h g^{-1})	charge capacity above 4.5 V (mA h g^{-1})	first charge capacity (mA h g^{-1})	first discharge capacity (mA h g^{-1})	first cycle efficiency (%)	first irreversible capacity loss (mA h g^{-1})
LLFNMO	181.8	184.9	366.7	252	68.7	114.7
AFCL	92.5	212.4	304.9	250.2	82.1	54.7
AOCL	150.7	207.6	358.3	272.3	76.0	86

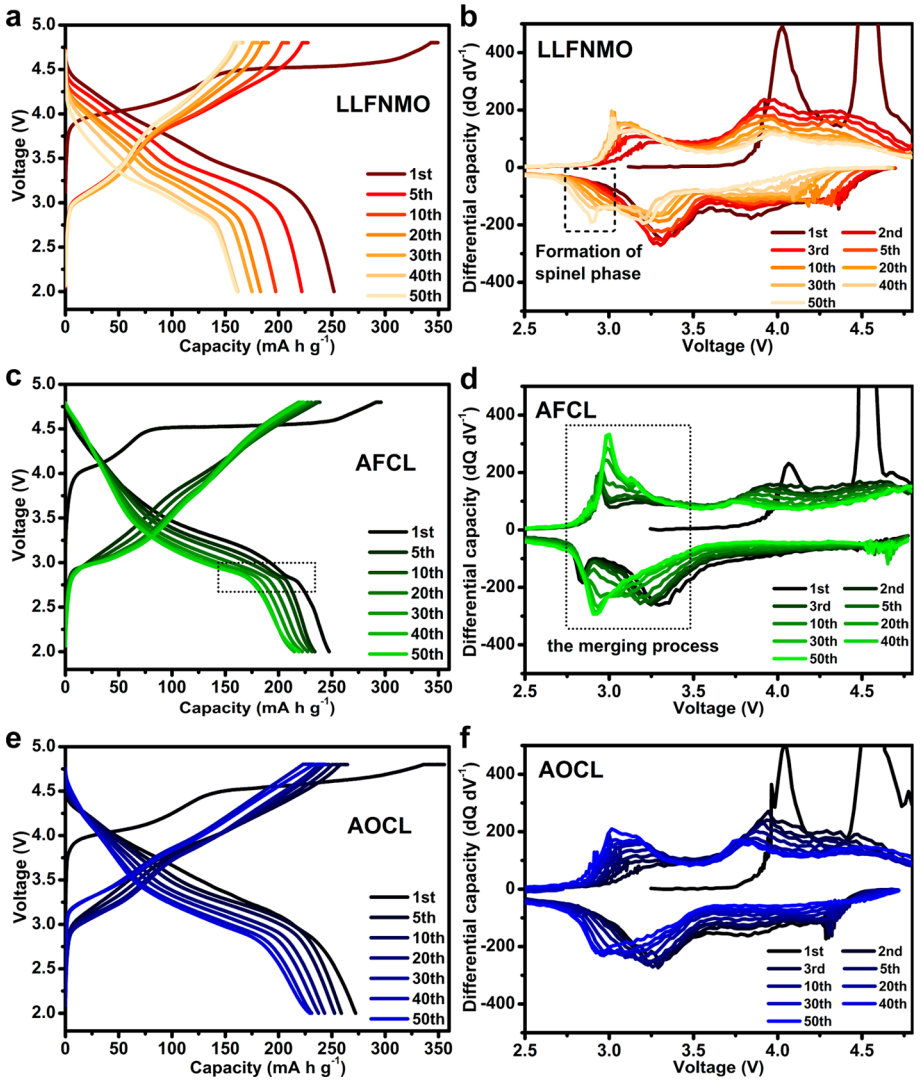

Figure 6. Charge/discharge curves at 0.1C and the corresponding dQ dV^{-1} versus voltage plots of all the samples.

calcination process at low temperature could give rise to the rearrangement of metal ions and to form other interesting and unexpected phase transition, which could be beneficial or harmful to the electrochemical performances. In the AFCL sample, it is speculated that the layer-to-spinel phase transformation was triggered by AlF_3 nanocoating during the calcination process, with extra lithium ions chemically leached from the Li-rich cathode.[26] When the lithium amount is reduced, the spinel component will be formed.

The first three charge/discharge curves cycled between 2 and 4.8 V at 0.1C and the corresponding differential capacity versus voltage plots (dQ dV^{-1}) of LLFNMO, AFCL, and AOCL are compared in Figure 5a. Similar to other Li-rich cathodes, all the cells exhibited two voltage plateaus around 4.0 and 4.5 V, corresponding to the extraction of lithium ions from layered structure and the extraction of lithium and oxygen from Li_2MnO_3 structure during the first charging process, respectively.[30,34] Obviously, the 4.0 V plateau of AFCL is much shorter than LLFNMO and AOCL, and a charge capacity of only 92.5 mA h g^{-1} was delivered. The charge capacity decreased with the increasing coating amount of AlF_3 (Figure S4 and Table S1, Supporting Information), due to the reduced Li-rich layered structure.[35] Furthermore, a 2.8 V reduction peak (black rectangle in Figure 5a), which is the characteristic peak of the spinel structure, appeared after the first charging process and gradually increased in intensity with increasing AlF_3 coating amount (Figure S4, Supporting Information), indicating the structure transformation induced by the AlF_3 nanocoating and in agreement with the previous XRD and TEM analysis. The oxidation peak of spinel phase was first observed from the

dx.doi.org/10.1021/am506934j | ACS Appl. Mater. Interfaces 2014, 6, 21711−21720

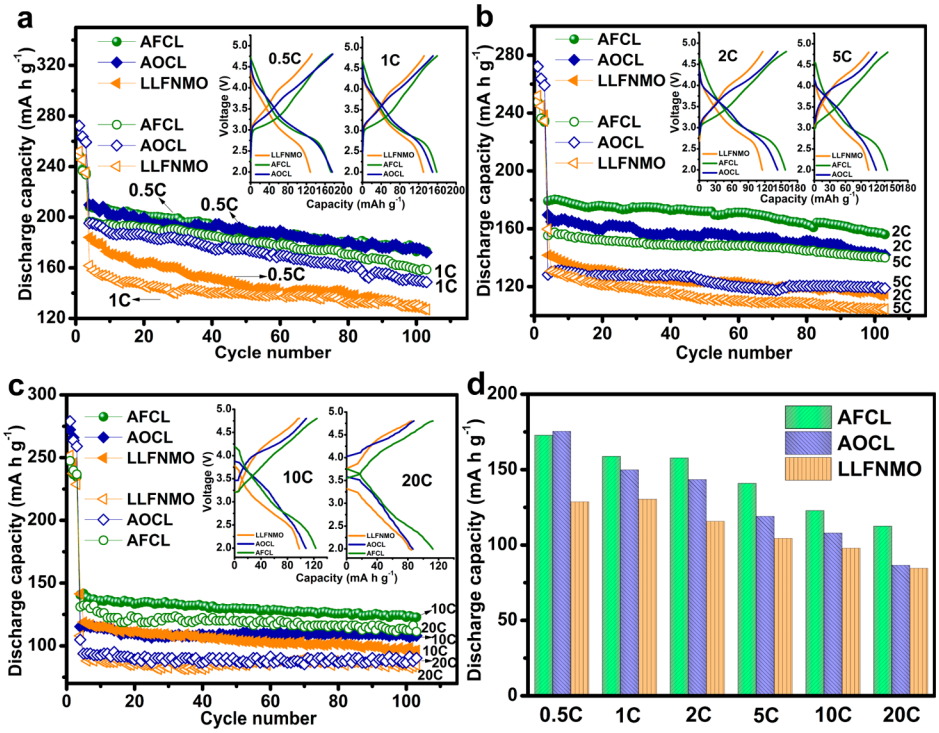

Figure 7. Rate capabilities from 0.5C to 20C, after activation under a charge/discharge rate of 0.1C for 3 cycles (a–c) and comparison of discharge capacities after 100 cycles (d). The 100th charge/discharge curves are inset in the corresponding graphs.

second charging process at 2.9 V (black rectangle in Figure 5a), indicating the good reversibility of spinel redox. As expected, this ~2.8 V peak cannot be observed from LLFNMO and AOCL. The 3.2 V reduction peaks observed from all the samples after the first charging process are believed to be the activation of Li_2MnO_3 phase, corresponding to the reduction of Mn^{4+} ions. In addition, reversible redox peaks at about 4.7 V are observed only in AFCL, which can be attributed to the $Ni^{2+/4+}$ in the induced spinel phase of high-voltage material $LiNi_xMn_{2-x}O_4$. Table 1 summarizes the specific capacities and cycle efficiencies at the first cycle for all the samples. Compared with the first discharge capacity (252 mA h g^{-1}) of LLFNMO, AOCL delivered a higher discharge capacity of 272.3 mA h g^{-1}, and AFCL exhibited a slightly lower discharge capacity of 250.2 mA h g^{-1}. Also, it can be seen that the charge capacity below 4.5 V in AFCL is much less than that of LLFNMO, in contrast to the comparison of charge capacity above 4.5 V, indicating that the layered component of $LiMO_2$ in the bulk material was transformed to spinel component of $LiNi_xMn_{2-x}O_4$ after AlF_3 coating. Although with the lowest first discharge capacity, AFCL showed the highest first Coulombic efficiency of 82.1% and the lowest irreversible capacity loss of 54.7 mA h g^{-1} (Table 1). In addition, the irreversible capacity loss reduced with the increasing coating amount of AlF_3, only 18.4 mA h g^{-1} for the 10 wt % AlF_3 coated sample (Table S1, Supporting Information). Figure 5b shows the cycling stability over 50 cycles of all the three samples tested between 2.0 and 4.8 V at 0.1C. AOCL sample delivered a much higher reversible capacity of 229.3 mA h g^{-1} and capacity retention of 84.2% than those of LLFNMO (164.8 mA h g^{-1} and 65.4%, respectively) after 50 cycles, due to the stabilization of the interface between the cathode and electrolyte. The reversible capacity (220 mA h g^{-1}) and capacity retention (87.9%) of AFCL sample were also superior to those of LLFNMO sample, ascribing to the stable cycling of the spinel $Mn^{3+/4+}$ in the 3 V and $Ni^{2+/4+}$ in the 4.7 V region as well as suppression of the surface side reaction and the low charge transfer resistance (Figure 5c).[36] Generally, the capacity of spinel phase is less than the corresponding layered phase, so the capacity of LLFNMO is reduced during cycling. By contrast, the high-voltage spinel phase induced by AlF_3 coating delivers higher capacity than the transformed spinel phase, so although the initial discharge capacity of AlF_3-coated sample is a little less than that of pristine sample, the capacity retention of AlF_3-coated sample is much higher than that of pristine one.

Charge/discharge curves of different cycles at 0.1C are displayed in Figure 6a, c, e. Obviously, the issue of voltage fading still presented in the three samples. Serious voltage fading along cycling was observed in LLFNMO sample, attributed to the continuous undesired layered-to-spinel phase transformation. However, the voltage fading rate of LLFNMO sample was effectively slowed down after the modifications by Al_2O_3 and AlF_3, as shown in Figure 5d. The integrated layered-spinel phase of AFCL sample is more beneficial for reducing the speed of voltage fading. Interestingly, independent spinel reduction peak at 2.8 V appeared after 20 cycles and grew up gradually during cycling in LLFNMO sample (Figure 6b), which may be due to the incompatibility between the initial layered structure and undesired spinel domains formed during cycling. For the AFCL sample (Figure 6d), the intensity of the redox peaks at 2.8 V gradually increased and shifted right with cycling and 3.3 V peaks shifted left at the same time. These two peaks merged into one peak finally and grew up gradually, indicating the harmonious coexistence of layered and spinel structures formed in synthesis process. This unique phenomenon was also observed when the charge/discharge rates are 0.5C and 1C (Figure S5, Supporting Information). Meanwhile, the redox peaks at 4.7 V become more apparent after 50 cycles,

dx.doi.org/10.1021/am506934j | ACS Appl. Mater. Interfaces 2014, 6, 21711–21720

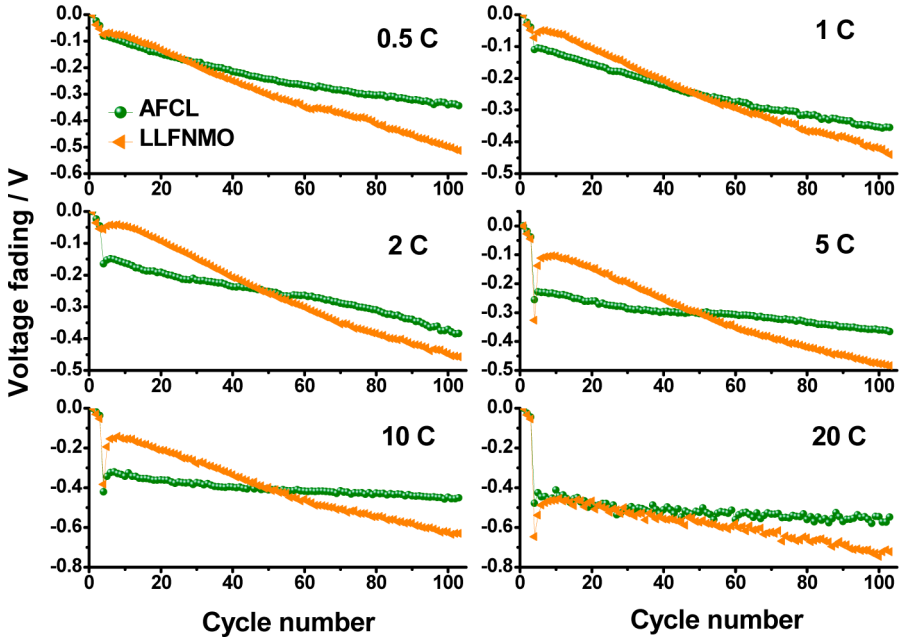

Figure 8. Comparison of voltage fading rates at different rates from 0.5C to 20C of LLFNMO and AFCL samples.

confirming the transformed spinel phase is high-voltage $LiNi_xMn_{2-x}O_4$ component in AFCL instead of the $LiMn_2O_4$ phase in the LLFNMO and AOCL. It can be concluded that although the combination of AlF_3 coating layer and integrated structures cannot ultimately stop the spinel formation, it can delay the phase transformation process.[35,37] The slowest rate of voltage fading and superior electrochemical stability of AFCL sample is tentatively attributed to a steadier arrangement of the layered- and spinel-like regions within the layered-spinel bulk structure as a result of a more stable electrode surface coating with AlF_3.[29] By contrast, the spinel phase formed during cycling in LLFNMO was unstable and therefore did not benefit for the electrochemical performances. It is noteworthy that the Al_2O_3 protective layer can also effectively slow down the formation rate of spinel phase (Figures 5d and 6f).

The rate capability from 0.5C to 5C after activation at 0.1C for 3 cycles highlights the advantages of AFCL sample. Clearly, AFCL and AOCL samples exhibited higher reversible capacity than LLFNMO sample at all rates (Figure 7). At 0.5C, there are no significant differences of the reversible capacity and the cycling stability between AFCL sample and AOCL sample. From 1C to 5C, AFCL sample showed the distinct advantage and the capacity gap between AFCL sample and AOCL sample progressively increased with rates. The reversible capacities after 100 cycles of AFCL sample were 172.8 mA h g^{-1} for 0.5C, 158.8 mA h g^{-1} for 1C, 157.7 mA h g^{-1} for 2C, and 140.9 mA h g^{-1} for 5C. The improved rate capability of AOCL sample are related to the less side reaction and lower charge transfer resistance compared to LLFNMO, while the fast kinetics of spinel phase transformation in AFCL together with the nanocoating improved its capability to transfer lithium ions at high rates.

To further highlight the good rate capability of AFCL sample, the cells were cycled at 10C and 20C between 2 and 4.8 V after the activation at 0.1C for 3 cycles. The typical charge/discharge curves are also shown in Figure 7. At 10C, AFCL sample delivered a reversible capacity of 122.8 mA h g^{-1} with retention of 87.3% after 100 cycles, which is higher than those of AOCL sample (108.5 mA h g^{-1}) and LLFNMO sample (97.9 mA h g^{-1}). AFCL sample had superior capacities at 20C as well. The reversible capacity of 112.5 mA h g^{-1} can still be obtained by AFCL sample, ascribed to its integrated structures and nanocoating. In addition, the suppression of the voltage fading at high rates can also be much improved by the integrated structures and nanocoating of AFCL sample, as shown in Figure 8. It can be seen that the fading voltage of AFCL sample is lower than that of LLFNMO sample after 100 cycles at all rates, indicating the better structural stability of the integrated layered-spinel material.

Consequently, the different microstructure of Al_2O_3 and AlF_3 coatings and spinel phase transformation in AOCL and AFCL have great influence on the electrochemical performances. Although the Li-rich layered component was reduced, AFCL sample still showed the superior electrochemical performances including the cycling and voltage stability and rate capability, which can be attributed to the ideal combination of stable integrated layered-spinel structures and the positive affection of the nanocoating. The high-voltage spinel phase in the host material induced by AlF_3 coating can provide 3D pathway for lithium ions transportation due to the fast kinetics of spinel phase transformation and compensate for the discharge capacity loss from the layered component. In addition, a steadier arrangement of the layered- and spinel-like regions within the layered-spinel bulk structure triggered by the AlF_3 coating could effectively reduce the voltage fading rate.

CONCLUSION

In conclusion, we applied the combination of phase transformation and nanocoating (AlF_3 and Al_2O_3) to Li-rich cathode $Li[Li_{0.2}Fe_{0.1}Ni_{0.15}Mn_{0.55}]O_2$ and developed a low-cost cathode with high rate capability and cycling stability for high-energy and high-power Li-ion batteries. The excellent electrochemical performances, including the improved cycling stability, the reduced first irreversible capacity loss, the outstanding high-rate capability, as well as the low voltage fading rate, demonstrated the positive roles of integrated layered-spinel structures and

nanocoating. In our opinion, the smart design of the effective combination should be developed on the other low-cost promising cathodes to realize both low cost and high performance for the next generation of Li-ion batteries.

■ ASSOCIATED CONTENT

Supporting Information

Compositional phase diagram of lithium−stoichiometric layered transition metal oxide: $LiFeO_2$−$LiNiO_2$−$LiMnO_2$, element mapping distributions of LLFNMO, AFCL and AOCL samples, XRD patterns of AlF_3 coated samples with different coating amounts, initial charge/discharge curves of the samples with different coating amounts of AlF_3 and the corresponding $dQ\ dV^{-1}$ vs voltage plots at 0.1C, the corresponding $dQ\ dV^{-1}$ vs voltage plots of different cycles for AFCL sample at 0.5C and 1C. This material is available free of charge via the Internet at http://pubs.acs.org.

■ AUTHOR INFORMATION

Corresponding Authors

*(R.C.) E-mail: chenrj@bit.edu.

*(F.W.) E-mail: wufeng863@bit.edu.cn.

Author Contributions

The manuscript was written through contributions of all authors. All authors have given approval to the final version of the manuscript.

Notes

The authors declare no competing financial interest.

■ ACKNOWLEDGMENTS

The experimental work of this study was supported by the Chinese National 973 Program (2015CB251100), the National Science Foundation of China (NSFC 51302014), Beijing Nova Program (Z121103002512029), Beijing Excellent Talents Plan funding, and the New Century Educational Talents Plan of the Chinese Education Ministry (NCET-12-0050). The authors would like to thank US-China Electric Vehicle and Battery Technology between China and the United States.

■ REFERENCES

(1) Lu, Z.; MacNeil, D. D.; Dahn, J. R. Layered Cathode Materials $Li[Ni_xLi_{(1/3-2x/3)}Mn_{(2/3-x/3)}]O_2$ for Lithium-Ion Batteries. *Electrochem. Solid-State Lett.* **2001**, *4*, A191−A194.

(2) Lu, Z.; Beaulieu, L. Y.; Donaberger, R. A.; Thomas, C. L.; Dahn, J. R. Synthesis, Structure, and Electrochemical Behavior of $Li[Ni_xLi_{1/3-2x/3}Mn_{2/3-x/3}]O_2$. *J. Electrochem. Soc.* **2002**, *149*, A778−A791.

(3) Kang, S. H.; Sun, Y. K.; Amine, K. Electrochemical and Ex Situ X-Ray Study of $Li(Li_{0.2}Ni_{0.2}Mn_{0.6})O_2$ Cathode Material for Li Secondary Batteries. *Electrochem. Solid-State Lett.* **2003**, *6*, A183−A186.

(4) Johnson, C. S.; Kim, J. S.; Lefief, C.; Li, N.; Vaughey, J. T.; Thackeray, M. M. The Significance of the Li_2MnO_3 Component in 'Composite' $xLi_2MnO_3\cdot(1-x)LiMn_{0.5}Ni_{0.5}O_2$ Electrodes. *Electrochem. Commun.* **2004**, *6*, 1085−1091.

(5) Barkhouse, D. A. R.; Dahn, J. R. A Novel Fabrication Technique for Producing Dense $Li[Ni_xLi_{(1/3-2x/3)}Mn_{(2/3-x/3)}]O_2$, $0 \leqslant x \leqslant 1/2$. *J. Electrochem. Soc.* **2005**, *152*, A746−A751.

(6) Johnson, C. S.; Li, N.; Lefief, C.; Thackeray, M. M. Anomalous Capacity and Cycling Stability of $xLi_2MnO_3\cdot(1-x)LiMO_2$ Electrodes (M = Mn, Ni, Co) in Lithium Batteries at 50 °C. *Electrochem. Commun.* **2007**, *9*, 787−795.

(7) Koenig, G. M.; Belharouak, I.; Deng, H.; Sun, Y. K.; Amine, K. Composition-Tailored Synthesis of Gradient Transition Metal Precursor Particles for Lithium-Ion Battery Cathode Materials. *Chem. Mater.* **2011**, *23*, 1954−1963.

(8) Zheng, J.; Gu, M.; Xiao, J.; Zuo, P.; Wang, C.; Zhang, J. G. Corrosion/Fragmentation of Layered Composite Cathode and Related Capacity/Voltage Fading During Cycling Process. *Nano Lett.* **2013**, *13*, 3824−3830.

(9) Gu, M.; Genc, A.; Belharouak, I.; Wang, D.; Amine, K.; Thevuthasan, S.; Baer, D. R.; Zhang, J. G.; Browning, N. D.; Liu, J.; Wang, C. Nanoscale Phase Separation, Cation Ordering, and Surface Chemistry in Pristine $Li_{1.2}Ni_{0.2}Mn_{0.6}O_2$ for Li-Ion Batteries. *Chem. Mater.* **2013**, *25*, 2319−2326.

(10) Arunkumar, T. A.; Manthiram, A. Factors Influencing the Irreversible Oxygen Loss and Reversible Capacity in Layered $Li[Li_{1/3}Mn_{2/3}]O_2$-$Li[M]O_2$ (M = $Mn_{0.5-y}Ni_{0.5-y}Co_{2y}$ and $Ni_{1-y}Co_y$) Solid Solutions. *Chem. Mater.* **2007**, *19*, 3067−3073.

(11) Zhao, T.; Chen, S.; Li, L.; Zhang, X.; Chen, R.; Belharouak, I.; Wu, F.; Amine, K. Synthesis, Characterization, and Electrochemistry of Cathode Material $Li[Li_{0.2}Co_{0.13}Ni_{0.13}Mn_{0.54}]O_2$ Using Organic Chelating Agents for Lithium-Ion Batteries. *J. Power Sources* **2013**, *228*, 206−213.

(12) Zhang, X.; Belharouak, I.; Li, L.; Lei, Y.; Elam, J. W.; Nie, A.; Chen, X.; Yassar, R. S.; Axelbaum, R. L. Structural and Electrochemical Study of Al_2O_3 and TiO_2 Coated $Li_{1.2}Ni_{0.13}Mn_{0.54}Co_{0.13}O_2$ Cathode Material Using ALD. *Adv. Energy Mater.* **2013**, *3*, 1299−1307.

(13) Tabuchi, M.; Nakashima, A.; Shigemura, H.; Ado, K.; Kobayashi, H.; Sakaebe, H.; Kageyama, H.; Nakamura, T.; Kohzaki, M.; Hirano, A.; Kanno, R. Synthesis, Cation Distribution, and Electrochemical Properties of Fe-Substituted Li_2MnO_3 as a Novel 4 V Positive Electrode Material. *J. Electrochem. Soc.* **2002**, *149*, A509−A524.

(14) Tabuchi, M.; Nabeshima, Y.; Ado, K.; Shikano, M.; Kageyama, H.; Tatsumi, K. Material Design Concept for Fe-Substituted Li_2MnO_3-Based Positive Electrodes. *J. Power Sources* **2007**, *174*, 554−559.

(15) Kikkawa, J.; Akita, T.; Tabuchi, M.; Shikano, M.; Tatsumi, K.; Kohyama, M. Formation and Disappearance of Spinel Nanograins in $Li_{1.2-x}Mn_{0.4}Fe_{0.4}O_2$ ($0 \leqslant x \leqslant 0.99$) during Extraction and Insertion of Li Ions. *J. Electrochem. Soc.* **2009**, *156*, A839−A845.

(16) Tabuchi, M.; Nabeshima, Y.; Takeuchi, T.; Tatsumi, K.; Imaizumi, J.; Nitta, Y. Fe Content Effects on Electrochemical Properties of Fe-Substituted Li_2MnO_3 Positive Electrode Material. *J. Power Sources* **2010**, *195*, 834−844.

(17) Kikkawa, J.; Akita, T.; Tabuchi, M.; Tatsumi, K.; Kohyama, M. Participation of Oxygen in Charge/Discharge Reactions in $Li_{1.2}Mn_{0.4}Fe_{0.4}O_2$: Evidence of Removal/Reinsertion of Oxide Ions. *J. Electrochem. Soc.* **2011**, *158*, A760−A768.

(18) Nakahara, K.; Tabuchi, M.; Kuroshima, S.; Toda, A.; Tanimoto, K.; Nakano, K. Drastically Improved Performances of Graphite/$Li_{1.26}Mn_{0.52}Fe_{0.22}O_2$ Cell with Stepwise Pre-Cycling Treatment that Causes Peroxide Forming. *J. Electrochem. Soc.* **2012**, *159*, A1398−A1404.

(19) Tabuchi, M.; Nabeshima, Y.; Takeuchi, T.; Kageyama, H.; Tatsumi, K.; Akimoto, J.; Shibuya, H.; Imaizumi, J. Synthesis and Electrochemical Characterization of Fe and Ni Substituted Li_2MnO_3—An Effective Means to Use Fe for Constructing "Co-Free" Li_2MnO_3 Based Positive Electrode Material. *J. Power Sources* **2011**, *196*, 3611−3622.

(20) Tabuchi, M.; Nabeshima, Y.; Takeuchi, T.; Kageyama, H.; Imaizumi, J.; Shibuya, H.; Akimoto, J. Synthesis of High-Capacity Ti- and/or Fe-Substituted Li_2MnO_3 Positive Electrode Materials with High Initial Cycle Efficiency by Application of the Carbothermal Reduction Method. *J. Power Sources* **2013**, *221*, 427−434.

(21) Karthikeyan, K.; Amaresh, S.; Lee, G. W.; Aravindan, V.; Kim, H.; Kang, K. S.; Kim, W. S.; Lee, Y. S. Electrochemical Performance of Cobalt Free, $Li_{1.2}(Mn_{0.32}Ni_{0.32}Fe_{0.16})O_2$ Cathodes for Lithium Batteries. *Electrochim. Acta* **2012**, *68*, 246−253.

(22) Uzun, D.; Doğrusöz, M.; Mazman, M.; Biçer, E.; Avci, E.; Şener, T.; Kaypmaz, T. C.; Demir-Cakan, R. Effect of MnO_2 Coating on Layered $Li(Li_{0.1}Ni_{0.3}Mn_{0.5}Fe_{0.1})O_2$ Cathode Material for Li-Ion Batteries. *Solid State Ionics* **2013**, *249−250*, 171−176.

(23) Zhao, T.; Li, L.; Chen, S.; Chen, R.; Zhang, X.; Lu, J.; Wu, F.; Amine, K. The Effect of Chromium Substitution on Improving Electrochemical Performance of Low-Cost Fe−Mn Based Li-Rich Layered Oxide as Cathode Material for Lithium-Ion Batteries. *J. Power Sources* **2014**, *245*, 898−907.
(24) Karthikeyan, K.; Amaresh, S.; Kim, S. H.; Aravindan, V.; Lee, Y. S. Influence of Synthesis Technique on the Structural and Electrochemical Properties of "Cobalt-Free", Layered Type $Li_{1+x}(Mn_{0.4}Ni_{0.4}Fe_{0.2})_{1-x}O_2$ ($0 < x < 0.4$) Cathode Material for Lithium Secondary Battery. *Electrochim. Acta* **2013**, *108*, 749−756.
(25) Li, J.; Wang, L.; Wang, L.; Luo, J.; Gao, J.; Li, J.; Wang, J.; He, X.; Tian, G.; Fan, S. Synthesis and Characterization of $Li(Li_{0.23}Mn_{0.47}Fe_{0.2}Ni_{0.1})O_2$ Cathode Material for Li-Ion Batteries. *J. Power Sources* **2013**, *244*, 652−657.
(26) Sun, Y. K.; Lee, M. J.; Yoon, C. S.; Hassoun, J.; Amine, K.; Scrosati, B. The Role of AlF_3 Coatings in Improving Electrochemical Cycling of Li-Enriched Nickel-Manganese Oxide Electrodes for Li-Ion Batteries. *Adv. Mater.* **2012**, *24*, 1192−1196.
(27) Lee, E. S.; Huq, A.; Chang, H. Y.; Manthiram, A. High-Voltage, High-Energy Layered-Spinel Composite Cathodes with Superior Cycle Life for Lithium-Ion Batteries. *Chem. Mater.* **2012**, *24*, 600−612.
(28) Lee, E. S.; Huq, A.; Manthiram, A. Understanding the Effect of Synthesis Temperature on the Structural and Electrochemical Characteristics of Layered-Spinel Composite Cathodes for Lithium-Ion Batteries. *J. Power Sources* **2013**, *240*, 193−203.
(29) Kim, D.; Sandi, G.; Croy, J. R.; Gallagher, K. G.; Kang, S. H.; Lee, E.; Slater, M. D.; Johnson, C. S.; Thackeray, M. M. Composite 'Layered-Layered-Spinel' Cathode Structures for Lithium-Ion Batteries. *J. Electrochem. Soc.* **2013**, *160*, A31−A38.
(30) Armstrong, A. R.; Holzapfel, M.; Novák, P.; Johnson, C. S.; Kang, S. H.; Thackeray, M. M.; Bruce, P. G. Demonstrating Oxygen Loss and Associated Structural Reorganization in the Lithium Battery Cathode $Li[Ni_{0.2}Li_{0.2}Mn_{0.6}]O_2$. *J. Am. Chem. Soc.* **2006**, *128*, 8694−8698.
(31) Thackeray, M. M.; Kang, S. H.; Johnson, C. S.; Vaughey, J. T.; Benedek, R.; Hackney, S. A. Li_2MnO_3-Stabilized $LiMO_2$ (M = Mn, Ni, Co) Electrodes for Lithium-Ion Batteries. *J. Mater. Chem.* **2007**, *17*, 3112−3125.
(32) Wu, F.; Li, N.; Su, Y.; Shou, H.; Bao, L.; Yang, W.; Zhang, L.; An, R.; Chen, S. Spinel/Layered Heterostructured Cathode Material for High-Capacity and High-Rate Li-Ion Batteries. *Adv. Mater.* **2013**, *25*, 3722−3726.
(33) Wu, F.; Li, N.; Su, Y.; Zhang, L.; Bao, L.; Wang, J.; Chen, L.; Zheng, Y.; Dai, L.; Peng, J.; Chen, S. Ultrathin Spinel Membrane-Encapsulated Layered Lithium-Rich Cathode Material for Advanced Li-Ion Batteries. *Nano Lett.* **2014**, *14*, 3550−3555.
(34) Kim, J. S.; Johnson, C. S.; Vaughey, J. T.; Thackeray, M. M.; Hackney, S. A.; Yoon, W.; Grey, C. P. Electrochemical and Structural Properties of $xLi_2M'O_3\cdot(1-x)LiMn_{0.5}Ni_{0.5}O_2$ Electrodes for Lithium Batteries (M′ = Ti, Mn, Zr; $0 \leqslant x \leqslant 0.3$). *Chem. Mater.* **2004**, *16*, 1996−2006.
(35) Myung, S. T.; Lee, K. S.; Yoon, C. S.; Sun, Y. K.; Amine, K.; Yashiro, H. Effect of AlF_3 Coating on Thermal Behavior of Chemically Delithiated $Li_{0.35}[Ni_{1/3}Co_{1/3}Mn_{1/3}]O_2$. *J. Phys. Chem. C* **2010**, *114*, 4710−4718.
(36) Sun, Y. K.; Myung, S. T.; Park, B. C.; Yashiro, H. Improvement of the Electrochemical Properties of $Li[Ni_{0.5}Mn_{0.5}]O_2$ by AlF_3 Coating. *J. Electrochem. Soc.* **2008**, *155*, A705−A710.
(37) Gu, M.; Belharouak, I.; Zheng, J.; Wu, H.; Xiao, J.; Genc, A.; Amine, K.; Thevuthasan, S.; Baer, D. R.; Zhang, J. G.; Browning, N. D.; Liu, J.; Wang, C. Formation of the Spinel Phase in the Layered Composite Cathode Used in Li-Ion Batteries. *ACS Nano* **2012**, *7*, 760−767.